Available online at www.sciencedirect.com
ScienceDirect
Journal of Nuclear Materials 367–370 (2007) 153–159
journal of nuclear materials
www.elsevier.com/locate/jnucmat

Lattice Monte Carlo simulations of nanocluster formation in nanostructured ferritic alloys

M.J. Alinger [a,b], B.D. Wirth [a,*], H.-J. Lee [a], G.R. Odette [b]

[a] Department of Nuclear Engineering, University of California, Berkeley, CA 94720-1730, USA
[b] Department of Materials, University of California, Santa Barbara, CA 93106-5070, USA

Abstract

Atom probe, electron microscopy and small angle neutron scattering data all indicate that nm-scale Y–Ti–O clusters precipitate from solid solution during high temperature consolidation of mechanically alloyed Fe–Cr–Ti–Y_2O_3 powders. These apparently coherent transition phases are precursors to equilibrium $Y_2Ti_2O_7$ pyrochlore oxides, and are distinguished by a low O/M ratio and lack of TEM diffraction contrast. In order to better understand the nature of these non-equilibrium features, Lattice Monte Carlo simulations of the nanocluster composition and structure were performed. The simulations used a rigid body-centered cubic lattice, with oxygen atoms placed on the octahedral interstitial sublattice, and considered variations in the cluster coherency strain, bulk composition and temperature. Pair bond energies were obtained from ab-initio calculations of the mixing enthalpies within a regular solution thermodynamics model. While the model is clearly oversimplified, the results provide helpful atomic-level insight into the Y–Ti–O nanoclusters and provide a basis for understanding the thermal and radiation stability. Future work will focus on including the effect of off-lattice relaxation and highly non-equilibrium vacancy concentrations on the precipitation kinetics.

1. Introduction

Nanostructured ferritic alloys (NFAs) are characterized by a very high number density dispersion of nm-scale Y–Ti–O rich phases [1,2]. These phases precipitate homogeneously during hot consolidation from highly supersaturated solid solutions produced by mechanical alloying Fe–Cr–Ti metallic powders (pre-alloyed or elemental) with Y_2O_3 [1,2]. Typical NFA compositions are ≈12–14 wt% Cr, 0.5 wt% Ti and 0.25 wt% Y. Atom probe [3], electron microscopy [4,5] and small angle neutron scattering [1,2] data all suggest that the smallest Y–Ti–O solute clusters are coherent transition phases, rather than equilibrium $Y_2Ti_2O_7$ pyroclore oxide phases. For typical alloy compositions, the number densities ($>10^{23}$–$10^{24}/m^3$) and size distributions of the nanoclusters (2–5 nm), as well as the balance of nanoclusters (NC) versus oxides, depends primarily on the consolidation temperature, typically 850–1150 °C [2]. Formation of the nm-scale clusters also requires Ti [1,2]. The NCs and oxides stabilize very fine grain sizes and subgrain dislocation structures of NFAs. As a result,

* Corresponding author. Tel.: +1 510 642 5341; fax: +1 510 643 9685.
E-mail address: bdwirth@nuc.berkeley.edu (B.D. Wirth).

0022-3115/$ - see front matter © 2007 Elsevier B.V. All rights reserved.
doi:10.1016/j.jnucmat.2007.03.010

NFAs have a very high tensile and creep [6,7] strength. It has also been shown that the NC are remarkably stable, coarsening and transforming to oxide phases only very slowly at temperatures less than 1000 °C [2].

It has also been proposed [8], and recently demonstrated [9], that the nanocluster interfaces can trap, and thus manage, high concentrations of transmutant helium in ultra fine-scale bubbles, that are associated with fusion and spallation proton irradiation environments. The NC and nanocluster-bubble complexes are also expected to enhance vacancy self-interstitial defect recombination rates, thus also mitigating displacement radiation damage. Further, it has been shown that NFAs have good ductility and are resistant to radiation induced loss of uniform strain capacity [10]. Finally, inclusion and coarse scale precipitate free, fine grained NFAs show promise of achieving good combinations of strength and fracture toughness, although additional research is needed optimize the balance of alloy properties.

In this work we address key questions regarding both the nature of, and factors that control, the chemistry and structure of the NC. For example, why do the NC form in preference to pyroclore oxides phases, which occur at only slightly larger sizes (>5–6 nm), and what controls their subsequent thermal and radiation stability. To this end we have carried out systematic atomistic lattice Monte Carlo (LMC) simulations of the NC. Our strategy is to compare the NC formed in the LMC to data from small angle neutron scattering (SANS) and atom probe tomography (APT) measurements to see if self-consistent structures and chemistries can be obtained. The SANS magnetic and nuclear scattering cross sections provides information on both the composition and atomic density of the NC, while the APT provides direct measures of their chemistries. A key issue is the NC and matrix strain energies that are required to maintain coherency with the Fe lattice.

2. Monte Carlo model and simulation technique

The key details of the atomistic model and the interaction (bond) energies used in the simulations are briefly summarized in this section. A more complete description of the interatomic potentials will be presented in a future publication.

Several simplifying assumptions are made regarding the alloy composition and the lattice structures simulated in the initial modeling. First, the chromium and tungsten do not play an obvious role in NC formation [1,2], and hence, are not included in the simulations. Therefore the alloy chemistry simulated is Fe–0.47 at.%Ti–0.12 at.%Y–0.19 at.%O. Second, since oxygen typically resides in octahedral interstitial lattice sites in iron, the simulation employs two sub-lattices (body-centered cubic, BCC and octahedral interstitial) to model the alloy system. Third, direct atom exchanges, instead of vacancy exchanges, are performed to minimize the system free energy. Thus no attempt is made to simulate the kinetic evolution of the NC, but rather the focus is on developing insight into the NC atomic configuration and composition.

The simulation cell has periodic boundary conditions and a specified number of solute atoms on rigid lattice sites, initially in a random solid solution. The simulation evaluates the exchanges of the solute atoms with their i ($i = 1$–8 for BCC and $i = 1$–4 for octahedral interstitials) first nearest neighbors (1NN) based on the Boltzmann weighted probabilities, P_i, defined as:

$$P_i = \exp\left(\frac{-\Delta E}{kT}\right) \quad \text{for} \quad \Delta E \geqslant 0 \text{ or } 1 \quad \text{for} \quad \Delta E < 0. \tag{1}$$

Here, E is the total system energy at a state and ΔE is the change in total system energy associated with each particular exchange. The probabilities are summed, normalized and a random number, R, between 0 and 1, is generated to determine which 1NN exchange is accepted, with the criteria that $P_{i-1} < R \leqslant P_i$. The solute atoms are randomly chosen (both sub-lattices) to make exchanges until all of the solutes have been exchanged during each MC sweep. Exchanges between like solutes are permitted to ensure every atom has moved at least once and to avoid forced dissolution of clustering atoms. Exchanges between sub-lattices are prohibited. However, both sub-lattices are considered when calculating ΔE. Thus the system evolves in a sequence of steps towards the lowest Gibbs free energy [11]. The LMC simulations are not intended to simulate NC evolution. Instead, they provide insight about the chemical structure of the NCs that cannot be determined from standard thermodynamic models.

An important and challenging aspect of the modeling effort is developing accurate descriptions of the atomic interactions. Since neither ab-initio derived,

nor embedded atom method (EAM) potentials for the constituents of this alloy are generally available, pair bond potentials have been used ($\varepsilon_{ii}, \varepsilon_{jj}, \varepsilon_{ij}$) within the general framework of regular solution theory. The potentials are evaluated at fixed lattice positions, and consider only first nearest neighbor bonds for metal–metal (Fe–Fe, Y–Y, Ti–Ti and Fe–Y, Y–Ti and Fe–Ti) interactions, first and second nearest neighbor bonds for metal–oxygen (Fe–O, Y–O and Ti–O) interactions, and up to fifth nearest neighbor bonds for oxygen–oxygen interactions. The potentials were derived from ab-initio calculations performed within the local density approximation (LDA) using the SEQUEST code [12], in addition to thermodynamic data approximated by regular solution theory. The LDA calculations of the potential energy per atom as a function of atomic volume and alloy concentration served as a basis for developing full potentials within Rose's equation of state [13] or the Lennard-Jones framework [14].

The bond energies between like atoms, ε_{ii}, were determined from the cohesive energies, E_{coh}, for the bcc phase of the pure elements. For the iron matrix, the cohesive energy was directly obtained from the literature [15]. For BCC yttrium and titanium, LDA calculations of the cohesive energy were performed as a function of atomic volume (lattice parameter), as shown in Fig. 1(a). The LDA results (shown as filled circles) have been fit to the Rose et al. equation of state [13] to obtain Y and Ti pair potentials (shown as the fit line) as a function of lattice parameter. For oxygen, the LDA calculations were performed for an oxygen (O_2) molecule as a function of bond length and the calculated cohesive energies were fit to a Lennard-Jones [14] functional to obtain an oxygen pair potential. Again, in this LMC model, the oxygen–oxygen interactions are included up to fifth nearest neighbor (on the octahedral interstitial sub-lattice), whereas the metallic elements are only included at first nearest neighbor positions.

The bond energies between different metallic atoms, ε_{ij}, were also obtained from LDA calculations of the potential energy of ordered BCC, 50% FeTi, YTi and FeY solid solutions as a function of lattice parameter (atomic volume), as shown in Fig. 1(b). Again, the LDA results are plotted as filled symbols and the lines are fits based on the Rose et al. equation of state [13]. Oxygen interactions with metallic Fe, Y or Ti (between octahedral interstitial and bcc sub-lattices) were modeled with bonds at both first and second nearest neighbor positions. The Fe–O bonds were estimated from CALPHAD data [16] for the free energy of the Fe–O system. The Ti–O and Y–O interaction potentials were fit to LDA calculations of a three atom unit cell as a function of lattice parameter. In these metal–oxygen LDA calculations, two metal atoms (Y or Ti) were placed on BCC lattice sites, while the single oxygen atom was placed on an octahedral interstitial site. Fig. 1(c) plots the LDA calculations of energy per atom for the Y–O, BCC Y and molecular oxygen as a function of lattice parameter (bond length for O_2), along with the corresponding full potential fits based on Rose's equation of state (Y–Y and Y–O) or Lennard-Jones functional forms.

As a first attempt to incorporate coherency strain size effects, the initial LMC simulations have been performed as a function of the NC lattice parameter for the oxygen–oxygen (O–O), metal–metal (Y–Y, Ti–Ti and Y–Ti) and oxygen–metal (Y–O and Ti–O) bonds within the nanoclusters, which effectively assesses the corresponding NC strain energy variations. The LMC simulations minimize the total system free energy at a self-selected average NC composition at the imposed atomic density.

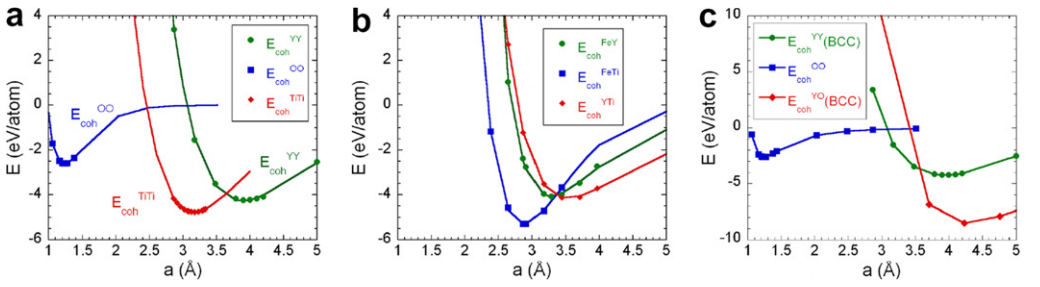

Fig. 1. LDA calculation results of the cohesive energy as a function of lattice parameter (data points) and fits (solid lines) to the LDA calculations based on Rose's equation of state (YY, TiTi, FeY, FeTi, YTi, YY, YO) or a Lennard-Jones functional form (O–O) for: (a) BCC Y, Ti and molecular O (as a function of bond length), (b) BCC Fe–Y, Fe–Ti and Y–Ti and (c) BCC Y, Y–O and molecular O.

Table 1
Pair bond energies (in eV) used in the LMC simulations as a function of lattice parameter aFe

Interaction	1.00aFe ε (eV)	1.15aFe ε (eV)	1.20aFe ε (eV)	1.25aFe ε (eV)	1.30aFe ε (eV)	1.35aFe ε (eV)
FeFe	−1.070	−1.070	−1.070	−1.070	−1.070	−1.070
YY	0.842	−0.635	−0.850	−0.981	−1.048	−1.068
TiTi	−1.049	−1.169	−1.110	−1.028	−0.933	−0.832
FeY	0.016	0.016	0.016	0.016	0.016	0.016
FeTi	−1.124	−1.124	−1.124	−1.124	−1.124	−1.124
YTi	−0.297	−0.984	−1.033	−1.037	−1.013	−0.970
OO(1NN)	−2.157	−1.390	−1.164	−0.964	−0.791	−0.643
OO(2NN)	−0.487	−0.179	−0.125	−0.086	−0.059	−0.039
OO(3NN)	−0.104	−0.024	−0.014	−0.008	−0.004	−0.002
OO(4NN)	−0.023	−0.003	−0.001	0.000	0.000	0.000
OO(5NN)	−0.004	0.000	0.000	0.000	0.000	0.000
FeO(1NN)	−0.422	−0.422	−0.422	−0.422	−0.422	−0.422
FeO(2NN)	−0.185	−0.185	−0.185	−0.185	−0.185	−0.185
YO(1NN)	9.676	0.105	−1.645	−2.919	−3.823	−4.442
YO(2NN)	4.233	0.046	−0.719	−1.277	−1.673	−1.943
TiO(1NN)	−1.717	−4.488	−4.964	−5.285	−5.482	−5.581
TiO(2NN)	−0.751	−1.964	−2.172	−2.312	−2.398	−2.442

The values for Fe–Fe, Fe–Y, Fe–Ti and Fe–O are kept constant at the value of 1.0aFe (0.287 nm), while those of Y–Y, Ti–Ti, Y–Ti, O–O, O–Ti, and Y–O are varied with lattice parameter to include the effect of lattice strain on the potential energy (bonding) between atoms within the nanocluster.

Lattice strain energies are not directly accounted for in the simulation, which may be an acceptable approximation for very small spherical clusters. However, the lattice energy is partly accounted for by imposing the Fe–Fe bond lengths on the dissolved O, Y and Ti solutes, rather than using their relaxed equilibrium Fe–M lengths. Note pair potentials also overestimate the energy of the atoms at the NC-matrix interface.

The various bond energies are presented in Table 1 as a function of lattice parameter. Along with the rigid lattice approximation, these values should be considered a crude, first order approximation for use in describing the energetics of the Fe–Y–Ti–O system; and more advanced models will be developed in the future. Nevertheless, this simplified description can accurately reproduce the alloy thermodynamics [17] and provides considerable atomic-level insight into the possible nanocluster structures and compositions.

3. Results and discussion

Fig. 2 shows characteristic NC structure, composition and size predicted by the LMC simulations of an Fe–0.47 at.%Ti–0.12 at.%Y–0.19 at.%O alloy, which has similar bulk Y, Ti and O concentration as MA957 and 12YWT [2,3], as a function of 'effective' NC lattice parameter at 273 K. While this is a very low temperature, similar results are observed at much higher temperatures as well. In these simulations, all of the O–O, Y–O, Ti–O, Y–Y, Ti–Ti, and Y–Ti bond energies were evaluated at the effective lattice parameter (e.g., $1.1a_o$), while the Fe–O, Fe–Fe, Fe–Y and Fe–Ti bonds always assume the value of the iron lattice, $a_o = 0.287$ nm. In this way, the effect of lattice strain on the potential energy (bonding) between atoms within the nanocluster can be included in minimizing the total system free energy, although again the detailed strain and strain energy partitioning to the matrix is not explicitely modeled. MC simulations performed using the full potential energy functions and without the requirement of the rigid lattice are currently being performed to assess the significance of structural relaxation at the interface and will be reported in the future.

The LMC simulations started from random solid solution in a $42 \times 42 \times 42$ unit cell containing 148 176 BCC (metal atom) sites (592 794 total lattice sites), with 696 Ti atoms, 178 Y atoms and 281 O atoms (on the octahedral interstitial lattice). Typically, several small clusters of Y, Ti and O rapidly form and subsequently coarsen to a single NC within about 5 million MC sweeps, as the potential energy of the system fluctuates towards a minimum value depending on simulation temperature. The single resulting NC corresponds to a precipitate

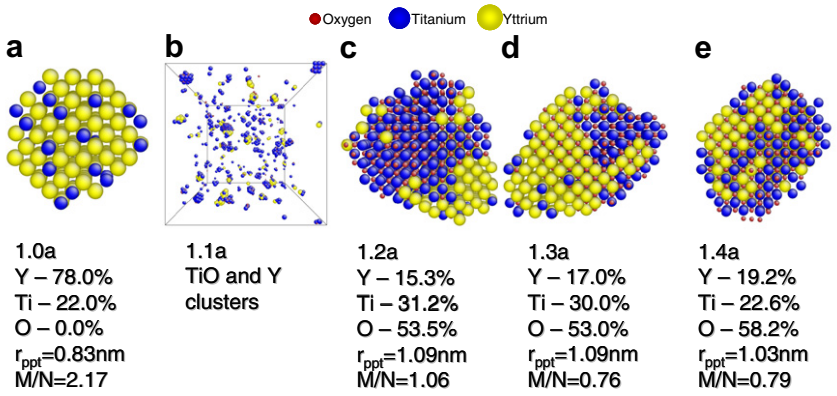

Fig. 2. LMC simulation results showing the predicted NC structure, size (precipitate radius, r_{ppt}), composition and calculated M/N scattering ratio as a function of NC lattice parameter (e.g., 1.0a, 1.1a, etc) in an Fe–0.47 at.%Ti–0.12 at.%Y–0.19 at.%O alloy at 273 K. Note that Y–Ti–O nanoclusters did not form with a NC lattice parameter of 1.1a, but rather individual TiO and Y clusters continually formed and dissolved, but did not coarsen into a single precipitate. Thus, the NC structure shown in (b) is different.

number density of 5.7×10^{23} m^{-3}, which is consistent with the experimentally observed number densities [1–3].

The Y–Ti–O nanoclusters in the NFAs MA957 and 12YWT have been extensively characterized by atom probe tomography (APT) [3] and small angle neutron scattering (SANS) [2] measurements, and key experimental results are summarized in Table 2 for comparison to the atomistic modeling results. The primary parameter from SANS is the magnetic to nuclear scattering ratio, which combines information of the composition and atomic density of the NC. The APT provides NC compositions, and especially the metal to oxygen ratio (M:O).

As shown in Fig. 2, Y–Ti–O nanoclusters do not form in the LMC simulations that assume a NC lattice parameter of $1.0a_o$ (a lattice match to the iron lattice) and $1.1a_o$. At a lattice parameter of $1.0a_o$, oxygen free precipitates form, with about 78%Y and 22%Ti. The Ti is segregated to the interface of these precipitates, for which we calculate a magnetic to nuclear (M/N) scattering ratio of ≈2.2. This M/N ratio is significantly higher than experimentally observed in MA957 and 12YWT that were processed at 1150 °C. In the case of a NC lattice parameter of $1.1a_o$, individual TiO and Y clusters form in the simulations, but Y–Ti–O NC do not form. Y–Ti–O NC do form at a NC lattice parameter = $1.2a_o$. These NC tend to be roughly spherical in shape, with segregated regions of Y and Ti and some segregation of Ti to the interface, and a more or less uniform oxygen concentration. The nanocluster formed at 1. $2a_o$ (Fig. 2(c)) has a calculated M/N ratio of ≈1.1 and a metal to oxygen ratio (M:O) of 0.9, which are reasonably consistent with the experimental M/N values between 0.9 and 1.2, and M:O ratios of 1.1–1.2. Increasing the effective NC lattice parameter above 1. $2a_o$ tends to increase the Y and decrease the Ti content of the NC at similar M:O ratios. However, the decreased Ti lowers the calculated M/N values below the experimentally observed range, and the trend in the Y/Ti ratio is opposite of the values observed by APT.

LMC simulations at higher temperatures of 673, 1273 and 1473 K and an effective NC lattice parameter of $1.2a_o$ produce similar nanocluster compositions and corresponding M:O and calculated M/N ratios. Fig. 3 shows the effect of increasing the bulk oxygen content of the simulated alloy from 0.25 to 1.5 at.%, at 673 K and a NC lattice parameter = $1.3a_o$. The resulting NC are slightly smaller (radii ≈ 0.7–0.9 nm) than those shown in Fig. 2. An increased alloy O content leads to decreased Y content and increased O content in the NC, at nearly constant Ti concentration. The corresponding M/N ratio increases with increasing O, while the metal to oxygen ratio decreases. Again, the

Table 2
Summary of APT [3] and SANS [2] data showing the NC composition, Metal–Oxygen (M:O) ratio and magnetic to nuclear (M/N) scattering ratio for MA957 and 12YWT

Alloy	Atom probe data				SANS data
	NC Composition (at.%)				
	Y	Ti	O	M:O	M/N
MA957	17.6	37.4	45.3	1.2	1.2
J12YWT	8.7	44.6	47	1.1	0.9

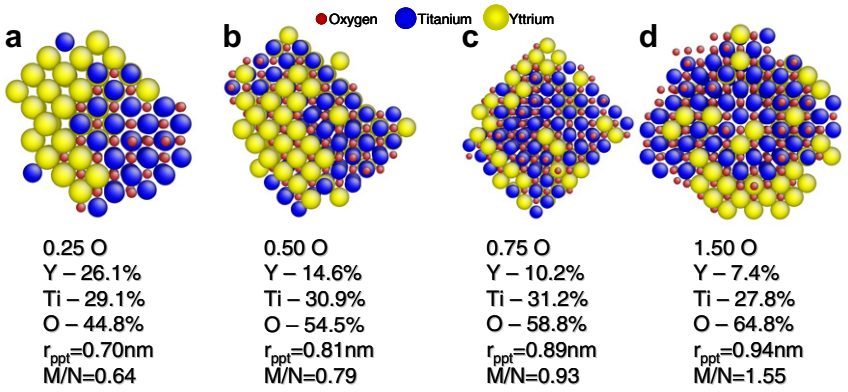

Fig. 3. LMC simulation results showing the predicted NC structure, size (precipitate radius, r_{ppt}), composition and calculated M/N scattering ratio as a function of alloy oxygen content in an Fe–0.47 at.%Ti–0.12 at.%Y alloy at 673 K and a NC lattice parameter of $1.3a_o$.

NCs consist of segregated Y and Ti rich regions, with a nearly uniform oxygen concentration. The decreasing Y content in the nanoclusters with increasing bulk O concentration may influence NC thermal stability, and is reasonably consistent with work by Ukai and co-workers where they found that excess O had a significant effect on the recrystallization temperature of NFAs [18].

Fig. 4 summarizes the LMC simulation results as a function of effective NC lattice parameter at 273, 673 and 1273 K (Fig. 4(a)) and as a function of matrix O concentration at 673 K and a NC lattice parameter = $1.3a_o$ (Fig. 4(b)). The simulation results show the Y, Ti and O content, the M/N and M:O ratio of the nanoclusters. APT and SANS characterization of MA957 and 12YWT indicated

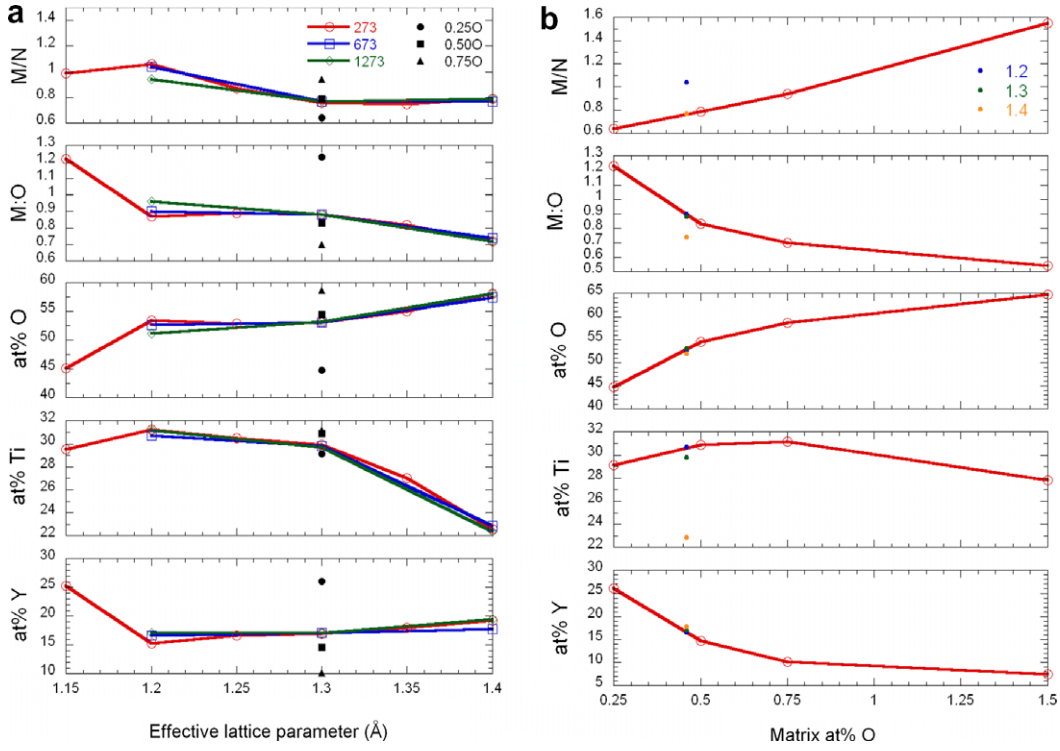

Fig. 4. Summary of the LMC simulation results (data points) showing the calculated M/N scattering ratio, Metal–Oxygen (M:O) ratio and NC composition as a function of (a) effective NC lattice parameter and temperature and (b) oxygen content and NC lattice parameter.

that the NC had average radii from 0.8 to 1.3 nm, metal to oxygen ratios of 1.1–1.2 with compositions of 9–18%Y, 37–45%Ti and 45–47%O and M/N scattering ratios of 0.9–1.2. The LMC results for NC lattice parameters between $1.2a_o$ and $1.3a_o$ are reasonably consistent with these experimental observations when the matrix O concentration is less than 0.5 at.%. The simulated NC are roughly spherical (faceted polyhedral), with segregated regions of Y and Ti, a slight enrichment of Ti at the interface, and a Ti to Y ratio of about 2:1, again reasonably consistent with the atom probe observations.

The best agreement between the LMC simulations and the experimental observations was found for a NC lattice parameter of $1.2a_o$–$1.3a_o$, indicating significant strain energy. Notably, large strain contrast has not been observed in TEM investigations of MA957 and 12YWT [19], which is not entirely understood. Future modeling efforts will investigate the partitioning of strain energy between the matrix and NC and the interfacial structure of the NCs by performing off-lattice relaxations using the full potential energy functions being developed in this work. Detailed understanding of the NC structure, composition and interface should provide additional insight into their thermal and irradiation stability, as well as their potential to trap He.

4. Conclusions and future work

A lattice Monte Carlo model for simulating the structure of Y–Ti–O nanoclusters in nanocomposited ferritic alloys has been presented. The bond energies (interatomic potentials) have been obtained from ab-initio calculations (within the local density approximation) of the mixing enthalpies in a regular solution thermodynamic model, fit to either Rose's equation of state or a Lennard-Jones functional form. LMC simulations performed in a Fe–0.47 at.%Ti–0.12 at.%Y–0.19 at.%O alloy, as a function of effective lattice parameter and temperature, reveal that Y–Ti–O nanoclusters form at all temperatures when the NC lattice parameter is larger than $1.2a_o$. The nanoclusters, with radii from 0.7 to 1.1 nm, are faceted polyhedrons of roughly spherical shape with compositions of 15–26%Y, 23–31%Ti and 45–65%O, and contain segregated regions that are Y or Ti rich, with nearly uniform O concentrations. The predicted NC for effective lattice parameters between $1.2a_o$ and $1.3a_o$ are reasonably consistent with the experimental observations when the matrix O concentration is less than 0.5 at.%. The correspondence with experimental observations at a relatively large lattice parameter indicates a significant strain energy contribution to the NC free energy. Future modeling efforts will investigate the partitioning of strain energy between the matrix and nanoclusters, and the interfacial structure by performing off-lattice relaxations using the full potential energy functions.

Acknowledgements

This work has been supported by the Office of Fusion Energy Sciences, US Department of Energy, under Grant DE-FG02-04ER54750 at UCB and Grant DE-FG02-04ER54275 at UCSB.

References

[1] M.J. Alinger, G.R. Odette, D.T. Hoelzer, J. Nucl. Mater. 329–333 (2004) 382.
[2] M.J. Alinger, PhD Dissertation, University of California, Santa Barbara, September 2004.
[3] M.K. Miller, E.A. Kenik, K.F. Russell, L. Heatherly, D.T. Hoelzer, P.J. Maziasz, Mat. Sci. Eng. A 353 (2003) 140.
[4] M. Klimiankou, R. Lindau, A. Moslang, Micron 36 (2005) 1.
[5] M. Klimiankou, R. Lindau, A. Moslang, J. Cryst. Growth 249 (2003) 381.
[6] B.N. Goshchitskii, V.V. Sagaradze, V.I. Shalaev, V.L. Arbuzov, Y. Tian, W. Qun, S. Jiguang, J. Nucl. Mater. 307–311 (2002) 783.
[7] R.L. Klueh, P.J. Maziasz, I.S. Kim, L. Heatherly, D.T. Hoelzer, N. Hashimoto, E.A. Kenik, K. Miyahara, J. Nucl. Mater. 307–311 (2002) 773.
[8] A. Kimura, R. Sugano, Y. Matsushita, S. Ukai, J. Phys. Chem. Sol. 66 (2005) 504.
[9] G.R. Odette, T. Yamamoto, J. Nucl. Mater., these Proceedings, doi:10.1016/j.jnucmat.2007.03.045.
[10] T. Yoshitake, Y. Abe, N. Akasaka, S. Ohtsuka, S. Ukai, A. Kimura, J. Nucl. Mater. 329–333 (2004) 342.
[11] D.A. Porter, K.E. Easterling, Phase Transformations in Metals and Alloys, Stanley Thornes, UK, 2000.
[12] http://dft.sandia.gov/Quest.
[13] J.H. Rose, J.R. Smith, F. Guinea, J. Ferrante, Phys. Rev. B 29 (1984) 2963.
[14] J.E. Lennard-Jones, Proc. R. Soc. London A 106 (1924) 463.
[15] C. Kittel, Introduction to Solid State Physics, John Wiley, New York, 1996.
[16] P.R. Subramanian, J.F. Smith, Calphad 8 (1984) 295.
[17] M.J. Alinger, B.D. Wirth, in: Fusion Materials Semi-Annual Progress Reports, DOE/ER-0313/38, 2005, p. 124.
[18] S. Ukai, T. Nishida, K. Kaneda, T. Okuda, M. Fujiwara, K. Asabe, S. Hagi, in: Symposium on Materials for Advanced Energy Systems and Fission and Fusion Engineering, vol. 108, 1996.
[19] D.T. Hoelzer, Personal communication, ORNL.